Functional insights into the mode of DNA and ligand binding of the TetR family regulator TylP from *Streptomyces fradiae*

Received for publication, March 23, 2017, and in revised form, July 21, 2017 Published, Papers in Press, July 24, 2017, DOI 10.1074/jbc.M117.788000

Shamayeeta Ray[‡§], Anwesha Maitra[‡], Anwesha Biswas[‡], Santosh Panjikar[¶‖], Jagannath Mondal[1], and Ruchi Anand[‡2]**

*From the [‡]Department of Chemistry, Indian Institute of Technology Bombay, Mumbai-400076, India, the [§]IITB-Monash Research Academy, Mumbai-400076, India, the [¶]Department of Biochemistry and Molecular Biology, Monash University, Victoria 3800, Australia, the [‖]Australian Synchrotron, Victoria 3168, Australia, and the **Tata Institute of Fundamental Research (TIFR) Centre for Interdisciplinary Sciences, Hyderabad-500075, India*

Edited by Chris Whitfield

Tetracycline repressors (TetRs) modulate multidrug efflux pathways in several pathogenic bacteria. In *Streptomyces*, they additionally regulate secondary metabolic pathways like antibiotic production. For instance, in the antibiotic producer *Streptomyces fradiae*, a layered network of TetRs regulates the levels of the commercially important antibiotic tylosin, with TylP occupying the top of this cascading network. TetRs exist in two functional states, the DNA-bound and the ligand-bound form, which are allosterically regulated. Here, to develop deeper insights into the factors that govern allostery, the crystal structure of TylP was solved to a resolution of 2.3 Å. The structure revealed that TylP possesses several unique features; notably, it harbors a unique C-terminal helix-loop extension that spans the entire length of the structure. This anchor connects the DNA-binding domain (DBD) with the ligand-binding domain (LBD) via a mix of positively charged and hydrogen-bonding interactions. Supporting EMSA studies with a series of ΔC truncated versions show that a systematic deletion of this region results in complete loss of DNA binding. The structure additionally revealed that TylP is markedly different in the orientation of its DBD and LBD architecture and the dimeric geometry from its hypothesized *Streptomyces* homologue CprB, which is a γ-butyrolactone regulator. Rather, TylP is closer in structural design to macrolide-binding TetRs found in pathogens. Supporting molecular dynamic studies suggested that TylP binds a macrolide intermediate in the tylosin pathway. Collectively, the structure along with corroborating biochemical studies provided insights into the novel mode of regulation of TetRs in antibiotic-producing organisms.

Tetracycline repressors (TetRs)[3] are the most prevalent class of transcription factors that are ubiquitously present in several antibiotic-resistant pathogens, where they control efflux of antibiotics out of the cell (1, 2). The founding member of this family, TetR, from which the name stems, regulates export of antibiotic tetracycline and thereby confers resistance to the bacteria harboring it (2). These receptors come in multiple forms: QacR and SmeT regulate multidrug efflux of a spectrum of antibiotics (1, 3), and TetR and ActR are pathway-specific regulators (1, 2). Bioinformatics analysis has revealed that the soil bacteria *Actinomycetes* generally contain a higher percentage of TetRs and employ these receptors to control multiple pathways associated with secondary metabolic functions (1, 4). In particular, bacteria of the *Streptomyces* genus are uniquely placed as they possess mechanisms not only to facilitate antibiotic resistance but also have the ability to produce them (5, 6). An evolutionary investigation reveals that most of the resistance mechanisms in pathogenic bacteria have stemmed from these ancient producer organisms and subsequently transferred across the species via lateral gene transfer (5, 7). Hence, TetRs from *Streptomyces* are the likely progenitors of TetRs found in resistant organisms (1).

Within the filamentous soil bacteria of *Streptomyces* genus, *Streptomyces fradiae* produces the commercially viable macrolide class of antibiotic, tylosin (8). Cundliffe and co-workers (9) have extensively studied the tylosin biosynthesis pathway and have assigned a hierarchical network of TetRs that regulate tylosin production. A combination of gene knock-out and RT-PCR experiments entailed that *S. fradiae* possesses a cluster of five different TetRs, TylS, TylR, TylU, TylP, and TylQ, that directly or indirectly affect tylosin production (10). Furthermore, it was additionally established that TylP is at the top of this cascading network and regulates the total concentration of tylosin in the cell (10). A TylP knock-out strain of *S. fradiae* substantially alters the control exhibited by this layered network, resulting in increased tylosin levels, thereby exposing the bacterium to enhanced antibiotic stress (9, 11). Based on

This work was supported by Department of Science & Technology (DST), Government of India, Grant EMR/2015/002121, Board of Research in Nuclear Sciences (BRNS), Government of India, Grant 37(1)/14/05/2017-BRNS/37039, Australia-India Council grant, and start-up funds provided by TIFR. The authors declare that they have no conflicts of interest with the contents of this article.

The atomic coordinates and structure factors (codes 5XAY and 5XAZ) have been deposited in the Protein Data Bank (http://wwpdb.org/).

This article contains supplemental Tables S1 and S2, Figs. S1–S9, Experimental procedures, and Results.

[1] Recipient of a Ramanujan fellowship provided by DST-SERB.

[2] To whom correspondence should be addressed: Structural Biochemistry Laboratory, Dept. of Chemistry, Indian Institute of Technology Bombay, Mumbai 400076, Maharashtra, India. Tel.: 022-576-7165; E-mail: ruchi@chem.iitb.ac.in.

[3] The abbreviations used are: TetR, tetracycline receptor; Se-TylP, selenomethionyl-TylP; DBD, DNA-binding domain; LBD, ligand-binding domain; GBL, γ-butyrolactone; PDB, Protein Data Bank; MD, molecular dynamics; r.m.s.d., root mean square deviation; HTH, helix-turn-helix; SAD, single-wavelength anomalous diffraction.

sequence similarity of TylP, it has been earlier proposed that TylP is a homologue of ArpA and CprB from *Streptomyces griseus* and *Streptomyces coelicolor,* respectively (9, 12, 13). These TetRs, instead of being triggered by antibiotics, are activated by small diffusible molecules, γ-butyrolactones (GBLs), that partake in a quorum-sensing cascade (14–17). However, as hypothesized previously, whether TylP accepts GBLs and thereby connects the antibiotic production pathways with the quorum-sensing ones still remains elusive.

X-ray structural analysis of TetRs reveals that they are Ω-shaped molecules and possess a modular architecture consisting of an N-terminal helix-turn-helix DNA-binding motif followed by a C-terminal bulkier domain that nests a ligand-binding site (1). Although the DNA-binding domain (DBD) is relatively conserved, the ligand-binding domain (LBD) is diverse in nature (1, 18). This is because the LBD is tailor made to respond to specific cues, and depending on the pathway a particular TetR regulates, the LBD evolves to fit the molecule of choice (19). For example, structural analysis of TetR bound to the antibiotic tetracycline shows that the pocket is relatively large, but in the case of CprB, which binds aliphatic carbon chain GBLs, the cavity is long and thin (16, 20). TetRs serve as transcription regulators by allosterically modulating the conformational states they span. Inside the cell, either they exist in a conformation conducive for DNA binding or adopt a state that can accommodate their cognate ligand. Because of the conformational restriction imposed, they are unable to simultaneously bind both the DNA and their cognate ligand of choice. They act as repressors in their DNA-bound form (1, 19); ligand binding, however, induces the release of the DNA, facilitating downstream transcription (1, 19). Select TetR structures in the ligand/DNA-bound and apo-forms provide clues into the mechanism of allostery (19–21). However, a generic evolutionarily conserved communication pathway that applies to this superfamily still remains elusive and requires the elucidation of more structural states in the requisite forms.

To develop functional insights into the mechanism of allosteric regulation, we have determined the structure of the TetR family regulator, TylP from *S. fradiae* to a resolution of 2.3 Å. TylP is the first structure of any TetR from *S. fradiae,* and surprisingly enough, it exhibits several distinctive features both in its DBD as well as the LBD. The most interesting structural finding is the presence of a unique C-terminal helix-loop extension, which directly interacts with the DBD. This feature is unique to TylP and provides a novel mode of regulation not yet discovered in any other TetR structures. Corroborating EMSA studies with a series of C-terminal truncated variants reveal that this anchor is essential for DNA binding and likely controls the allosteric states accessed by TylP. Additionally, the structure also provides clues into the cognate ligand of TylP. MD studies in conjunction with fluorescence quenching and isothermal calorimetric studies reveal that contrary to its annotation as a GBL, TylP does not respond to it. MD results indicate that it binds a polyketide intermediate in the tylosin biosynthesis pathway and thereby controls tylosin production. Overall, the structure of TylP opens new avenues toward a broader understanding of the regulation of DNA binding and antibiotic biosynthesis in this class of TetRs.

Table 1
Crystallographic data statistics

Processing	Se-TylP (PDB code 5XAY)	Native (PDB code 5XAZ)
Wavelength (Å)	0.968	0.968
Resolution (Å)	19.9–2.6	19.8–2.3
Space group	$P2_1$	$P2_1$
Unit cell	$a = 101.3$, $b = 71.8$, $c = 160.1$ $\alpha = \gamma = 90°$, $\beta = 102.5°$	$a = 101.5$, $b = 71.6$, $c = 158.6$ $\alpha = \gamma = 90°$, $\beta = 102.9°$
Mosaicity (°)	0.11	0.21
Total reflections	291,224/46,371	345,824/34,873
Unique reflections	69,940/11,014	98,807/8942
Multiplicity	4.1/4.2	3.5/3.9
Completeness(%)	99.5/98.4	99.7/96.1
$I/\sigma(I)$	8.6/2.9	14.9/2.8
R_{merge} (%)	13.2/54.2	11.0/40.7
R-meas (%)	15.1/62.1	12.7/48.1
Refinement		
Total no. of non-hydrogen atoms	12,805	13,826
Total no. of protein atoms	12,673	13,358
Total no. of water atoms	132	468
No. of reflections in refinement	69,922	97,167
No. of reflections in test set	994	992
R factor (%)	22.8	20.4
R_{free} (%)	28.4	25.2
Bonds (Å)	0.02	0.02
angles (degree)	1.9	1.9
Most favored region (%)	94.9	95.2
Additional allowed region (%)	4.6	4.1
Disallowed region (%)	0.5	0.6
Mean B factors (Å^2) for overall structure	34.7	33.1

[a] $R_{merge} = \Sigma_{hkl}\Sigma_i|I_i(hkl) - \langle I(hkl)\rangle|[BAR]/\Sigma_{HKL}\Sigma_i I_i(hkl)$.
[b] R-meas($R_{r.i.m.}$) $= \Sigma_{hkl}(N/(N-1))^{1/2} \times \Sigma_i|I_i(hkl)\langle I(hkl)\rangle|\Sigma_{hkl}\Sigma_i I_i(hkl)$, where $I_i(hkl)$ is the ith intensity measurement of reflection hkl, $\langle I(hkl)\rangle$ its average, and N is the multiplicity of a given reflection. Values after the / are for the high resolution shell.

Results and discussion

Structure solution

Diffraction quality crystals of TylP were obtained in two different conditions (as detailed under "Experimental procedures"). Initial attempts to solve the crystal structure using CprB as a molecular replacement template failed. The structure was subsequently determined by selenomethionine SAD phasing to an initial resolution of 2.6 Å (PDB code 5XAY) (Table 1). Using this structure as a search model, molecular replacement was performed with native TylP, and the structure was refined to a higher resolution of 2.3 Å (PDB code 5XAZ) (Table 1). Each asymmetric unit of TylP includes four identical dimers (supplemental Fig. S1). Briefly, in each dimeric unit, one of the subunits (subunit B) exhibits continuous density for residues 4–216; however, the last 10 amino acids are disordered. However, in subunit A, the density for residues corresponding to 68–72 is missing, and the rest of the structure including the C-terminal tail (residues 217–226) is ordered. Each subunit consists of 11 helices organized in two domains arranged sequentially from the N to the C terminus (Fig. 1*A* and supplemental Fig. S2*A*). The root mean square deviation (r.m.s.d.) between both the subunits is 1.34 Å, with the largest differences corresponding to the alternate missing loops in the LBD and the DBD in both the subunits (Fig. 1*B* and supplemental Fig. S2*B*).

Overall structure

TylP has an overall architecture that resembles other TetRs; however, it has several significant structural features that make it rather unique and probably help accomplish its function. It possesses the typical Ω-shaped structure with the N-terminal

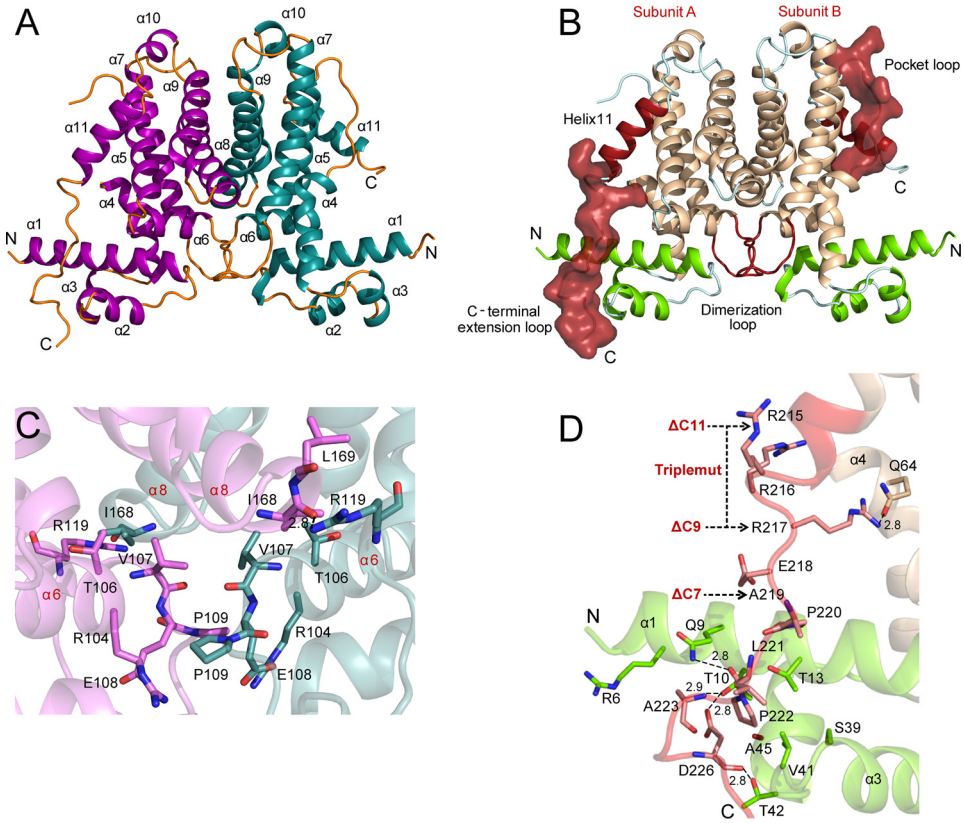

Figure 1. Structural analysis of TylP. *A,* structure of TylP dimer highlighting the secondary structural elements, with α-helices in *purple* (*subunit A*) and *deep teal* (*subunit B*), and the loop regions are in *orange*. *B,* TylP dimer highlighting the unique regions is in *red*. The rest of the LBD of both subunits are represented in *wheat*, and the DBD is *green*. The regions that are exclusively present in only one subunit are represented as a *red surface*. *C,* zoomed view of the dimerization loops from both subunits showing all the interacting residues in *stick* representation, which are present at the loop interface. Carbon atoms of the residues of subunit A are in *violet* and that of subunit B are in *teal*. *D,* magnified view of the interactions of the extended C-terminal loop (in *red*) with the DBD (in *green*) and α4 (in *wheat*). Carbon atoms of the loop residues are in *salmon*, the DBD residues are in *green,* and α4 are in *wheat*. The regions involved in all the truncated constructs have been highlighted with *dotted lines*. *C* and *D*, oxygen atoms are represented in *red* and nitrogen in *blue*.

DNA-binding domain (DBD) possessing the conventional helix-turn-helix motif. Of the first three α-helices comprising the DBD, helices α2–α3 typically partake in DNA binding and insert themselves into the major groove of the DNA, whereas α1 communicates with the ligand-binding domain (Fig. 1*A*). Examination of the structure reveals that TylP has a rather long N-terminal helix, which consists of several arginine residues and a tandem array of alanine residues. In many other TetRs like SimR and CgmR, these N-terminal extensions play a critical role in enhancing DNA binding via interaction of the positively charged region with the minor groove of the DNA (22, 23). In TylP, this extension runs across the entire length of the HTH motif and most probably is important for stabilizing the DNA-bound form as well as in conferring selectivity toward its cognate DNA.

The ligand-binding domain of TylP includes eight core helices. It has several distinctive insertions in this domain (Fig. 1*B* and supplemental Fig. S3). Overall, it was observed that as compared with other TetRs, the LBD of TylP has more regions, which instead of folding into helices form ordered loops. For example, the C-terminal helix (α10) that caps the ligand-binding pocket is rather short in TylP. Unlike other TetRs, such as CprB, SmeT, QacR, etc., instead of forming a long helix this region adopts a loop conformation. Additionally, this loop region connects into an adjacent helix (α11), which is unique to TylP (Fig. 1*B*). In comparison with other TetRs, the connector helix α4 between LBD and DBD is also shorter. This helix connects into a flexible loop (pocket loop), spanning residues 68–76, that acts as a flap on one side of the LBD and exhibits clear density in the subunit B but is in a disordered state in the other subunit (Fig. 1*B* and supplemental Fig. S3*B*). This pocket loop along with select residues from helices α4, α5, α7, and α8 primarily comprises the ligand-binding region of the subunit B, creating a pocket volume of 450 $Å^3$. Because the loop region is disordered in subunit A, the apparent pocket volume is 795 $Å^3$ in this subunit (as calculated by CastP server) (24).

The dimeric interface of TylP is essentially hydrophobic in nature and is formed by the juxtaposition of primarily helices α6, α7, and α8 from each subunit. A few interactions from α9 also partake in the dimer formation. The interface has a combined buried surface area of 1486 $Å^2$ with 20 amino acids interacting between the subunits. The dimeric interface is "V"-shaped and is tethered at the base via hydrogen bonding contacts (Fig. 1*C*). For example, the guanidinium headgroup of Arg-119, which lies at the start of α7 from subunit A, interacts with the backbone of Ile-168 that forms the last turn of α8 from subunit B. Additionally, the loop spanning residues 108–117 that connects α6 and α7 from each subunit are stacked together via a Pro-109 residue. These loops intertwine to form a butterfly-shaped structure establishing a communication channel

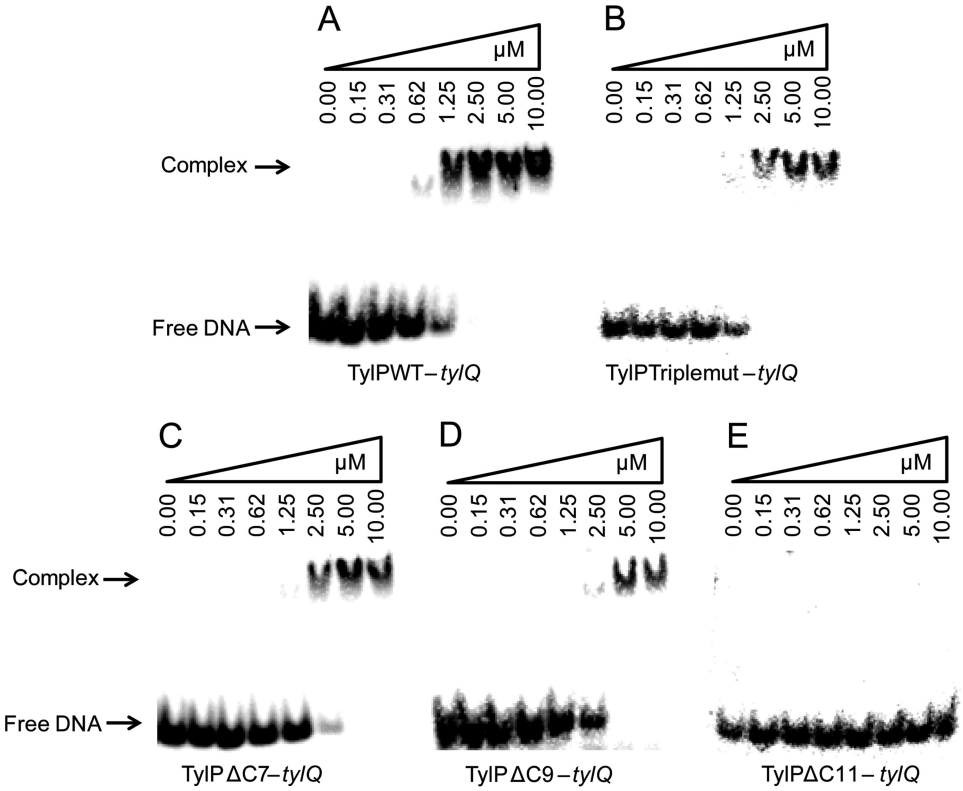

Figure 2. Role of the exclusive C-terminal loop in DNA binding. *A,* EMSA of wild-type TylP (*TylPWT*) and C-terminal extension truncated versions; *B,* TylP Triplemut (arginine residues 215–217 mutated to alanine); *C,* TylPΔC7 (last 7 residues deleted); *D,* TylPΔC9 (last 9 residues deleted); and *E,* TylPΔC11 (last 11 residues deleted) with a reported 44 mer *tylQ* DNA. Concentrations of the proteins are mentioned in micromolar range, and the free DNA and complex are indicated. Systematic deletion of the C-terminal loop leads to gradual abolishment of DNA binding.

between the two monomers. This stabilizing feature is unique to TylP. In other TetRs, either this region is flexible or the loop length is shorter impeding any interaction.

A very distinctive feature of TylP is the presence of an unusually long unique C-terminal helix-loop extension, including 12 amino acids, that runs along the length of the structure and interacts with the DNA recognition helices α1 and α3 as well as the connector helix α4 (Fig. 1, *B* and *D*). This loop is well defined in subunit A but is consistently disordered in subunit B in all four dimers of the asymmetric unit (supplemental Figs. S1 and S3*A*). A close examination of this region shows that this loop is anchored via hydrogen bonding and hydrophobic interactions at several positions by the DNA-binding helices (Fig. 1*D*). For instance, the amide nitrogen atom of residue Gln-9 from α1 interacts with the backbone carbonyl of Leu-221 of the loop. Similarly, the side chain hydroxyl group of Thr-10 from α1 forms hydrogen-bonding interactions with the acid headgroup of Asp-226 along with the amide nitrogen atom of Ala-223. Additionally, the hydroxyl group of Thr-42 from α3 also seals this interaction by hydrogen bonding with peptidyl carbonyl of Asp-226. Pro-220 and Pro-222 further strengthen the interface by making hydrophobic interactions with residues of the helix α1. Another feature of the C-terminal anchor is the presence of an arginine-rich stretch (residues 215–217). In the apo structure, the guanidinium nitrogen atom of one of the arginines, Arg-217, interacts with the carbonyl oxygen atom of Gln-64 from the connector helix α4 (Fig. 1*D*). This positive stretch probably undergoes a conformational change on DNA binding and likely helps stabilize the interaction of TylP with the DNA. Thus, the C-terminal extension bridges the DBD and the LBD likely establishing a communication channel between them.

Insights into regulation of the DBD via the C-terminal extension

To better understand the role played by the unique C-terminal helix-loop extension that establishes a link between the two modular domains, this region of the protein was altered, and the variants were biochemically studied. The major question perceived here was whether this extension plays an important role in allosteric regulation of the DBD. The extension region forms contacts with the DNA-binding HTH motif via its last 10 residues (Fig. 1*D*). Hence, several truncated versions of TylP were constructed that include ΔC7 (lacking the last 7 residues), ΔC9 (lacking the last 9 residues), and ΔC11 (lacking the last 11 residues). Prior to further experimentation, proper folding of the truncated proteins was confirmed by performing circular dichroism with the wild-type (WT) and all the mutant constructs (supplemental Fig. S4). Subsequently, to gauge the effect of the C-terminal extension on the DNA-binding ability of TylP, EMSA of the WT and the truncated proteins was carried out with a representative 44-mer *tylQ* promoter sequence (Fig. 2). It was observed that the binding affinity of WT TylP with the *tylQ* sequence was around 1 μM (Fig. 2*A*). In contrast, EMSA of the ΔC7 and ΔC9 versions with the *tylQ* DNA exhibited a gradual reduction in DNA-binding ability by 3- and 5-fold, respec-

tively (Fig. 2, *C* and *D*). For the ΔC11 truncation, a complete loss of DNA binding was observed (Fig. 2*E*). Moreover, as mentioned earlier, the C-terminal tail of TylP possesses an array of three tandem arginine residues. Because in several DNA-binding proteins the positively charged residues have been shown to partake in stabilizing the negative phosphate backbone of the DNA, the role of the C-terminal arginines of TylP was also explored. EMSA on a triple mutant version of TylP, where the three arginine residues 215–217 were mutated to alanine (Triplemut), exhibited a 3-fold loss in *tylQ* DNA-binding ability (Fig. 2*B*). All these results clearly show that the C-terminal extension plays a crucial role in allosterically regulating the DNA-binding ability of the TylP DBD.

We propose that the regulation of the DBD by the C-terminal extension could be via two possible scenarios. One instance could be that upon DNA binding the C-terminal anchor of TylP completely rearranges itself and directly interacts with the DNA, and the existing conformation, which the apo crystal structure presents, is no longer adopted. Another possibility is that the current crystal structure is not completely hypothetical and offers a glimpse into the actual mode of interactions of the DBD with the DNA. The structure perhaps presents a hybrid state, with subunit A, where the extension anchors the DBD and facilitates DNA binding, representing a picture closer to the DNA-bound form. Whereas subunit B, in which the C-terminal region is disordered but the LBD pocket loop is ordered, is a gross representation of the ligand-bound form. The EMSA results partially support this conjecture and are in tune with the structural data. Close examination of the interactions of the C-terminal extension with the N-terminal DBD in the crystal structure discloses that maximum contacts occur in the extreme C-terminal tail region (residues 220–226), with the upstream residue Arg-217 forming a salt bridge with the connector helix α4, further sealing the interface. The systematic results from EMSA studies show that both the C-terminal tail as well as the upstream arginine cluster contribute equally toward binding. This is evident from the fact that substitution of the three upstream arginine residues in the extension results in only a partial reduction in the DNA-binding ability of TylP (Fig. 2*B*). Moreover, the structure reveals that having the last seven amino acids of the tail deleted (ΔC7 construct) results in loss of four hydrogen-bonding interactions and corroborating EMSA exhibits a significant loss in DNA binding (Fig. 2*C*). This is despite the fact that the ΔC7 still harbors the three positively charged residues. Together, loss of both the arginine cluster as well as the tail region (ΔC11 construct) seems to be essential for complete abolishment of the DNA binding (Fig. 2*E*). Overall, we hypothesize that the C-terminal extension plays a dual role, it not only anchors the DBD via a mix of hydrogen bonding and hydrophobic interactions but also stabilizes the DNA–protein interaction by presenting a positively charged interface.

Comparison of TylP with other TetRs

To gain further functional insights, structural homologues of TylP were determined using the DALI server taking the monomer as a search model. *S. coelicolor* GBL-binding protein CprB was the top hit with a *Z* score of 19.1 and an overall r.m.s.d. of 3.6 Å for 196 residues aligned (16, 20). Other proteins that also showed high DALI scores include the multidrug efflux pump repressor SmeT, which binds triclosan and induces antibiotic resistance in *Stenotrophomonas maltophilia* (3, 25), and MtrR, from *Neisseria gonorrhoeae* that regulates macrolide efflux leading to antimicrobial resistance (26). FadR, which is a TetR regulator involved in the fatty acid degradation, also showed significant structural homology with TylP and was one of the top DALI hits (27).

CprB exhibits 80% sequence identity with TylP in the DBD region (supplemental Fig. S5). In lieu of this high sequence homology in the DBD of TylP and CprB, an LSQab superposition (28) of the HTH motifs was performed. Although at the monomeric level, the DBDs of the two proteins align really well (r.m.s.d. of 0.9 Å for 48 Cα atoms of subunit B, Fig. 3*A*), it was observed that in a dimeric setting only one of the HTH motifs of TylP aligns with the HTH of CprB. In the other monomer (subunit A), the TylP DBD adopts an orientation such that there is no overlap between the HTH motifs. This DBD in TylP was found to adopt a state such that it is positioned at an angle of 30° above the CprB dimeric axis (Fig. 3*A*). This indicates that despite having the highest sequence identity in this region, the conformational and structural orientations of the DBD of TylP and CprB in their apo-forms are quite different.

Furthermore, structural comparison of the DNA-bound and apo-forms of CprB showed that conformation of the DBD in the apo-form was a close representation of the DNA-bound state of the protein (20). This was also apparent from the minimal change in the distance between the recognition helices (measured from the amine nitrogen atom of the second residue in the recognition helix α3 of each monomer of the dimer) of the two forms of CprB (the α3–α3′ distance being 38.2 and 40.2 Å for the DNA-bound and the apo-form, respectively) (Fig. 3*B*). However, in the apo-TylP structure, this distance was 51.6 Å. Scrutiny of other TetRs reveals that the change in the α3–α3′ distance between the apo- and DNA-bound forms exhibits a broad pattern across TetRs (Fig. 3*B*). For instance, in another dimer of dimer TetR, TM1030, this distance changed drastically from 53.9 Å in the apo-form to 36.2 Å in the DNA-bound form (29). However, a pattern that emerges from the analysis is that for all TetR–DNA complexes, even after distortions induced upon DNA binding, this α3–α3′ distance is in the range 30–40 Å (30). In the case of TylP, a value of 51.6 Å in the apo structure indicates that the current X-ray crystallographic state is not close to a DNA-bound form, and a major conformational change needs to occur to facilitate DNA binding. As proposed previously, the apo-form of the protein is likely a hybrid state that neither fully represents the DNA-bound or the ligand-bound form. Instead, we believe that based on the stimuli, it is primed to swing in either direction. We speculate that in the DNA-bound state, both the C-terminal anchors become ordered in the dimer, and this structural rearrangement facilitates the event of DNA binding. A DNA–protein crystal structure, however, will be needed to determine the DNA-binding mechanism of TylP at the molecular level.

Because TylP was theorized to be a GBL receptor and the GBL binder CprB, although being its top DALI hit, exhibited disparity at the DBD dimeric organization, we decided to investigate further structural similarities and differences of the two

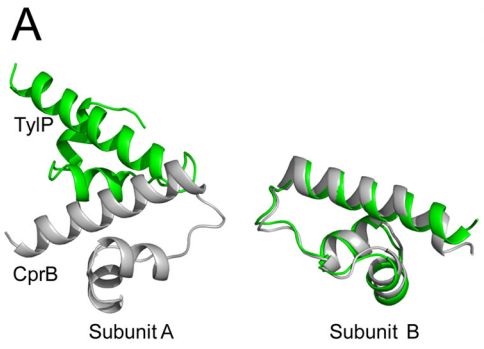

B

Protein	DNA bound	Apo
	Distance (α3-α3'), Å	
HrtR	32.1	31.3
TetR	30.4	35.2
SimR	32.4	39.8
AmtR	32.6	40.5
KstR	33.9	47.5
Ms6564	35.4	21.1
QacR	37.0	36.0
CprB	38.2	40.2
SlmA	37.0	43.0
TM1030	36.2	53.9
TylP	-	51.6

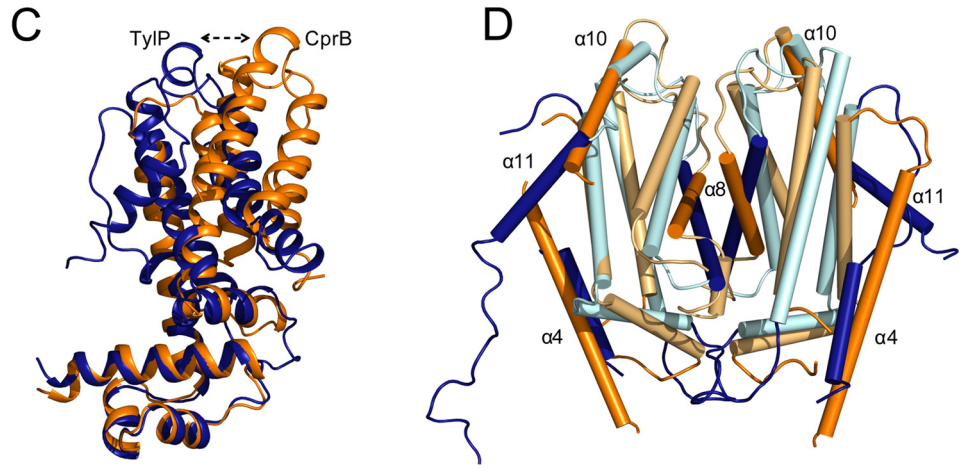

Figure 3. Structural comparison of TylP with other TetRs. *A,* superposition of the HTH DBD of the dimeric form of TylP (in *green*) and CprB (in *gray*). *B,* distances between the HTH motifs of a dimer of the apo and DNA-bound forms of different TetRs are listed. The rows in *light green* correspond to the dimeric DNA binding TetR-FTRs and in *blue* correspond to the dimer of dimer DNA-binding sub-class, and the row representing TylP is in *red*. The PDB codes and the chain IDs of the apo and the DNA-bound structures used to measure the DBD distances have been listed in supplemental Table S1. *C,* superposition of monomers of TylP (in *deep-blue*) and CprB (in *orange*) highlighting the shift in angle of the LBDs. *D,* superposition of TylP and CprB LBD in dimer form. The regions which show maximum differences in TylP and CprB, are highlighted in *deep-blue* and *orange*, respectively.

proteins. Monomer alignment of the unliganded structures of TylP and CprB revealed that a superposition of the DBDs results in offset of the LBDs. The result clearly shows that the orientation of the LBD with respect to the DBD is distinctly different in the two proteins with the DBD to LBD angle being 69 and 90° in TylP and CprB, respectively (Fig. 3*C* and supplemental Fig. S6*A*). Furthermore, a comparison of the LBD and DBD angles of TylP with a subset of TetRs revealed that the interdomain angle of TylP is closest to MtrR, with CprB being the most aberrant and FadR and SmeT angles being in between (supplemental Fig. S6*A*). This analysis insinuates that TylP maybe functionally analogous to macrolide-binding TetRs like MtrR.

In addition to the monomeric forms, the biological dimer architecture of TylP was also probed. TylP dimer, composed of only the LBDs, was superimposed with CprB and a spectrum of other TetRs. The results show that the dimeric orientation and contact between CprB and TylP are markedly dissimilar (Fig. 3*D*). For instance, the orientation of the key helix (α8, from each subunit) at the dimeric interface is completely different, and the secondary structural elements are directed such that an oppositely oriented "V"-shaped interface is created in both the structures. In CprB, the top portion of α8 from both subunits is anchored, whereas in TylP, the interface is strengthened at the bottom end. Furthermore, the butterfly-shaped dimerization loop region of TylP exclusively strengthens the base (Fig. 3*D*). Overall, it was observed that the LBD of TylP faces away from the dimeric interface, but in CprB the LBD faces toward it. As a result, the TylP dimer is less compact than CprB, and the overall breadth of TylP with respect to CprB is greater by ~5 Å. The broader width of TylP hints that it can exhibit more conformational flexibility and thereby can probably prime itself to accommodate larger ligands in comparison with CprB. A broader search among other TetRs further reveals that the general LBD architecture and dimerization geometries of TylP are the closest to macrolide-binding proteins like MphR(A) and MtrR (supplemental Fig. S6*B*). Overall, all these structural comparisons suggest that TylP demonstrates organizational similarities with other macrolide-binding proteins. Therefore, the potential ligand of TylP might not be a GBL moiety but a macrolide.

Ligand-binding pocket of TylP

To obtain more detailed information about the nature of the ligand recognized by TylP, the pocket residues were identified using CASTp server (Fig. 4*A*). The residues that line the pocket consist of residues Ile-81, Thr-85, and Leu-88 from α5; Trp-125, His-128, Gly-129, Leu-132, and Leu-133 from α7; Ala-152, Leu-155, Val-156, and Phe-159 from α8; and His-183 from α9 that form one side. The other face is capped by the flexible loop region that contributes Val-68, Pro-69, Pro-70, and Pro-71, as well as Gln-64 and Leu-65, from α4. Both Trp-125 and His-128

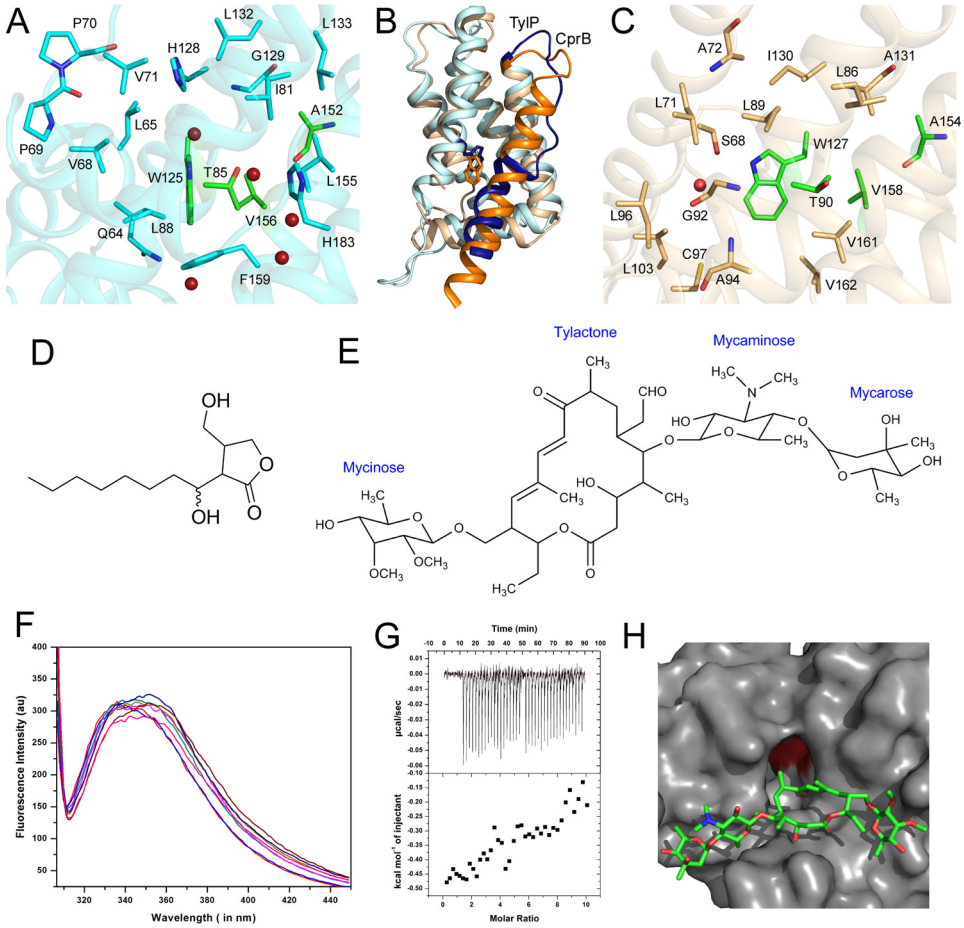

Figure 4. Analysis of ligand-binding pocket of TylP. *A* and *C*, pocket architecture of TylP (*A*) and CprB (*C*) highlighting all the ligand-binding residues in *stick* representation. The carbon atoms of unique residues of TylP are in *cyan* and that of CprB are in *wheat*. The conserved residues in both are in *green*, and oxygen and nitrogen are in *red* and *blue*, respectively. The water molecules in both the pockets are represented as *red spheres*. *B,* superposition of LBD of monomer of TylP and CprB highlighting the variable regions in *deep blue* (TylP) and *orange* (CprB). *D* and *E* represent 2D structure of a synthesized GBL (*D*) and tylosin antibiotic (*E*). *F,* fluorescence quenching studies of TylP with the synthesized GBL. *G,* isothermal titration calorimetry of TylP with tylosin, where the curves that correspond to raw data are shown in the *top panel* and the curve fit in the *bottom panel*. *H,* docking of TylP (represented as *gray* surface highlighting the binding pocket, and conserved tryptophan residue is highlighted in *red*) with tylsoin (in *stick* representation with carbon, oxygen, and nitrogen atoms colored in *green, red,* and *blue*, respectively).

divide the pocket along its length. Additionally, it was noticed that the pocket harbors five water molecules that hydrogen-bond with the hydrophilic side groups of select amino acids (Fig. 4*A*). To evaluate whether the TylP pocket could potentially bind a GBL, the pockets of CprB and TylP were compared. Superposition of only the LBD domains of the monomers of both the proteins were performed to facilitate alignment of this region, and it was noticed that both the proteins harbor the conserved tryptophan residue Trp-127 in CprB and Trp-125 in TylP (Fig. 4*B*). Apart from this apparent conserved residue, there are many differences in the overall pocket architecture. For instance, the flap region closing onto the pocket is dissimilar between the two proteins. The CprB pocket is more constricted with its long α4 helix lining the pocket entrance along with a small flap. The opening for the pocket in TylP consists of an extended loop region with the α4 becoming shorter, thereby allowing more flexibility to the pocket to potentially accommodate larger size ligands (Fig. 4*B*). Furthermore, analysis shows that although the pocket of CprB is very hydrophobic (Fig. 4*C*) which can facilitate binding of molecules like GBLs (which contain extended aliphatic chain appendages), the TylP pocket environment is more hydrophilic and can probably accept more amphipathic ligands. Attempts to dock GBLs in the TylP pocket also failed. Even fluorescence quenching experiments with a synthesized GBL (Fig. 4*D*) yielded negative results (Fig. 4*F*). Therefore, the possibility of GBLs being the potential ligands of TylP appears to be a rather remote option.

In lieu of the fact that TylP plays an important role in the regulation of tylosin biosynthesis (9, 12), the possibility of tylosin (Fig. 4*E*) being its potential ligand was explored. However, docking studies revealed that tylosin is too bulky to fit into the TylP ligand-binding pocket (Fig. 4*H*). Furthermore, supporting isothermal calorimetry experiments and DNA breaking assay using EMSA also negate this hypothesis (Fig. 4*G* and supplemental Fig. S7). Therefore, the option of TylP accepting smaller tylosin fragments (or pathway intermediates) like tylactone or tylactone with sugar was explored.

MD simulation studies of TylP

In several TetRs, substantial changes in the ligand-binding pocket volume as well as conformation of the LBD occur upon ligand binding (21, 25). Therefore, MD simulations on the

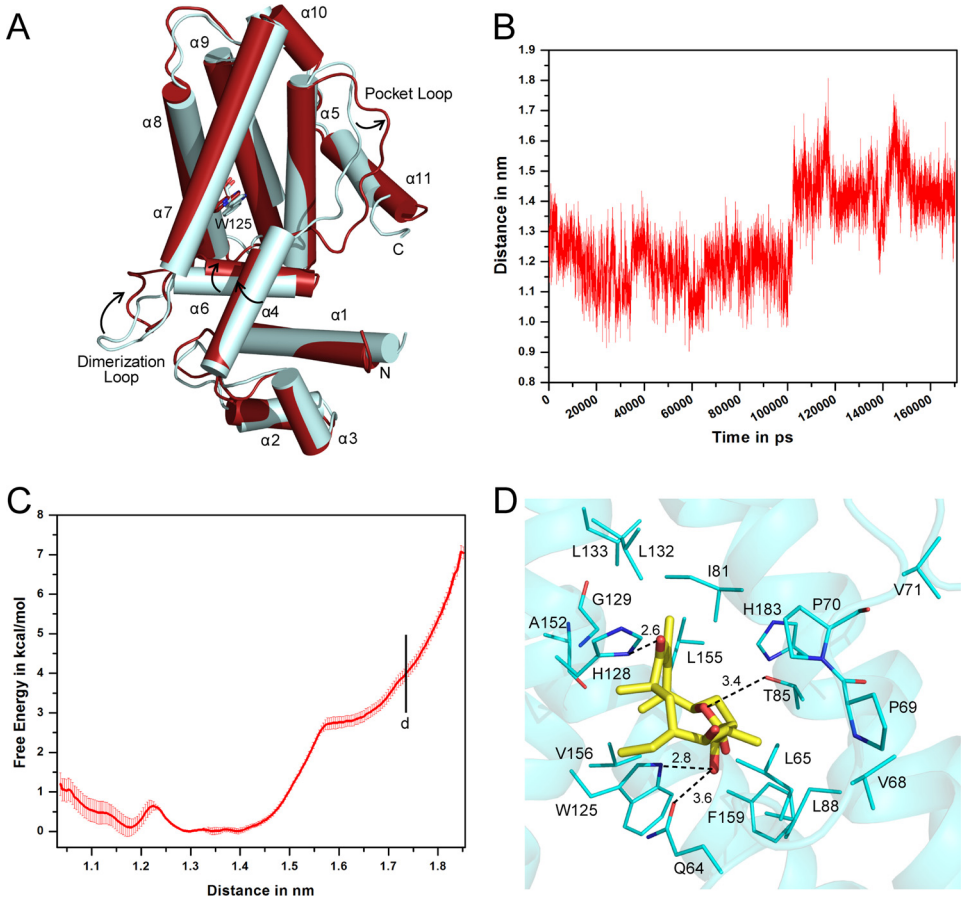

Figure 5. Molecular dynamic simulation studies of TylP. *A,* superimposed structures of native TylP (in *gray*) and TylP conformation obtained after MD simulation (in *red*). All the helices have been *numbered*, and the shifts in both the structures have been shown with a *black arrow*. Trp-125 is represented as a *stick* in both structures. *B,* distance plot between Trp-125 and pocket loop (consisting of residues Ala-67 to Val-71). *C,* free energy plot for different conformations of TylP at room temperature (303.15 K). TylP conformation corresponding to the highlighted distance *d* (1.733 nm) docked best with tylactone. *D,* ligand-binding pocket of MD generated TylP (at 144,580 ps). The carbon atoms of the pocket residues are in *cyan* and those of tylactone are in *yellow*. Oxygen atoms are represented in *red* and nitrogen in *blue*.

native protein system were performed to map potential intermediate conformations of TylP that might be suitable to accommodate the ligands. The trajectories from regular MD simulation on TylP at a slightly higher temperature (313.15K) and at room temperature (303.15K) were both analyzed to identify energetically favorable states (detailed in the supplemental material). Superimposition was performed between the initial X-ray structure of TylP and the favorable conformations at different snapshots captured from these simulations (Fig. 5*A*). Consequently, conformations where distances between the center of the masses of the pocket loop residues and tryptophan (Trp-125) on helix 7 were found to vary significantly (1.1–1.8 nm at 313.15 K) during the course of simulation, were chosen for further analysis (Fig. 5*B*). Umbrella sampling was performed to confirm that these states are accessible at room temperature *i.e.* 303.15K (supplemental Fig. S8). It was found that multiple conformations of TylP can exist at room temperature where the pocket volume is such that ligand binding can be facile. From the selected snapshots, docking studies were performed using AutoDock (31), and it was ascertained that tylactone, the tylosin intermediate, is the most preferred ligand (supplemental Table S2). The state (144.580 ns) corresponding to distance 1.733 nm (*d* in Fig. 5*C*) was additionally found to be most apt for tylactone binding as it exhibited a favorable change in free energy (ΔG) and maximum population in a single cluster. It was noted that this state has an enlarged pocket volume of 707 $Å^3$ as compared with 446 $Å^3$ in the initial TylP structure. As mentioned before, this increase in pocket size on ligand binding is not a surprising revelation and has been observed in other TetRs (21, 25).

In the snapshot of TylP taken at 144.580 ns of MD simulation, it was observed that the macrolide is stabilized by a mix of hydrophobic and hydrogen bonding contacts (Fig. 5*D*). The macrolide moiety has several hydroxyl and carbonyl groups that serve as anchors and stabilize it in the TylP pocket (Fig. 5*D* and supplemental Fig. S9). For example, the OH group at the C4 position of the macrolide hydrogen bonds with both the indole nitrogen atom of Trp-125 from α7 and the side chain carbonyl group of Gln-64 from α4. Similarly, O1 in the tylactone ring is also engaged in hydrogen bonding contact with the side chain hydroxyl group of Thr-85 from α5. Additionally, the carbonyl group at the C10 position of tylactone interacts with the imidazole side chain of His-128 from α7 (Fig. 5*D* and supplemental Fig. S9). The mix of hydrophilic and hydrophobic interactions observed in the TylP–tylactone complex is reminiscent of the binding pattern observed in other antibiotic-binding TetRs like

MphR(A) and tetracycline receptor TetR. For instance, in MphR(A), the hydroxyl groups of the macrolide ring of erythromycin is stabilized by the hydrophilic side chain residues like histidine, serine, and asparagine (2, 32). Overall, the MD analysis indicates that the TylP pocket is designed to potentially accommodate a macrolide moiety.

The MD studies also provide clues into the conformational changes in the LBD of TylP from the apo-state (captured by crystallography) to the final ligand-bound form (achieved after simulation). Notably, ligand binding results in reorientation of the pocket loop, which creates space for the macrolide tylactone to bind (Fig. 5*A*). Simultaneously, it appears that α6 and α4 also reorient such that they come closer to α1, thereby mediating the event of ligand binding to the HTH motif. Another striking feature is the dramatic change in conformation of the exclusive dimerization loop present at the base of the interface (Fig. 5*A*). This butterfly-shaped loop seems to be dynamic during the course of the simulation, and results indicate that it partakes in enhanced communication between the two subunits upon ligand binding, thereby transmitting the presence of the ligand across the dimers.

Overall, this study provides important insights into the functional role of TylP in *S. fradiae*. The apo structure has opened doors toward identifying the unique mode of regulation of its DBD, via its C-terminal extension. It also breaks the dogma of TylP being a GBL receptor. Rather, it appears that TylP is a macrolide-binding protein that plays an important role in antibiotic regulation. As a future direction, the pressing need would be to solve the structures of TylP with cognate DNA as well as with the identified potential ligands. Ongoing efforts in our laboratory are proceeding in this direction.

Experimental procedures

Cloning and protein purification

S. fradiae strain harboring the *tylP* gene (obtained from Prof. Eric Cundliffe, University of Leicester) was grown and harvested using standard protocol (33), and the genomic DNA was subsequently isolated from it using the standard CTAB method (34). The purified genomic DNA of *S. fradiae* (1 μg/μl) was used as a template for the PCR amplification of the full-length *tylP* gene that encodes 226 amino acid residues. The amplified *tylP* gene was cloned into pET28a expression vector, using NcoI-XhoI restriction site combination, which adds a C-terminal His tag to the protein. Using the native TylP gene as a template, the following C-terminal truncated clones of *tylP* were made similarly as described above, ΔC7 (lacking the last 7 residues), ΔC9 (lacking the last 9 residues), and ΔC11 (lacking the last 11 residues). A triple mutant, Triplemut (arginines 215–217 mutated to alanine), was also cloned in a similar manner. The wild-type *tylP* and all the C-terminal modified/truncated expression constructs were subsequently transformed into *Escherichia coli* BL21(DE3) Rosetta cells, overexpressed with 0.3 mM isopropyl β-D-thiogalactopyranoside as His_6 tag fusion proteins, and purified using nickel-nitrilotriacetic acid resin by standard His-tagged affinity purification protocol. Purification details of the native, mutated, and selenomethionyl-TylP (Se-TylP) is provided in supplemental Experimental procedures.

Crystallization, data collection, processing, and refinement of TylP

The purified His-tagged native and Se-TylP (10 mg/ml) were first screened for crystallization using several commercially available crystallization screens, and crystals appeared within a week in the following conditions: (*a*) 0.1 M sodium citrate tribasic dihydrate (pH 5.6), 2% v/v tacsimate (pH 5.0), 16% w/v PEG 3350, and (*b*) 0.2 M ammonium citrate tribasic (pH 7.0), 20% w/v PEG 3350. Under optimized conditions, native and Se-TylP crystallized in the monoclinic space group $P2_1$ with unit cell dimensions of $a = 101.33$ Å, $b = 71.88$ Å, and $c = 160.06$ Å and $\alpha = \gamma = 90°$ and $\beta = 102.54°$. Each asymmetric unit contains eight monomers that correspond to a calculated solvent content of 55%. X-ray diffraction experiments were performed at the micro-focus beamline (MX2) of the Australian Synchrotron. A single crystal of each of native and Se-TylP was cryoprotected with 15% (v/v) glycerol (prepared using mother liquor) prior to data collection. Se-TylP crystal was flash-cooled in liquid nitrogen and transferred to a stream of nitrogen gas at 100 K. A 2.6 Å resolution SAD data set for Se-TylP was collected at 0.9686 Å wavelength using an ADSC Quantum 315 CCD detector. 200 diffraction images with 1° oscillation width were collected with the crystal-to-detector distance 380 mm. The X-ray diffraction data for the native TylP was collected and processed similarly as described above (data statistics depicted in Table 1). The structure of Se-TylP was solved at 2.6 Å using the SAD protocol of Auto-Rickshaw (35) (PDB code 5XAY) (refer to supplemental Experimental procedures for details). The crystal structure of native TylP was solved at a higher resolution of 2.3 Å (PDB code 5XAZ) by the molecular replacement method using the MR protocol of Auto-Rickshaw and Se-TylP as a search model. Manual model building of the partially refined structures was carried out using the graphics program COOT (36), and they were further refined using REFMAC5, including NCS restraints and TLS refinement. Both the structures were validated by performing rotamer, geometry, and density fit analysis using COOT (36), and the Ramachandran outliers were less than 1% in the final refined structures. All the data refinement statistics are summarized in Table 1. All figures were made in PyMOL (37).

Radiolabeling of oligonucleotide

A 44-mer *tylQ* DNA (5′-GTTGACCGTATACAAACCGCGTCAGCGGTTTGTAAAATCCCGCG-3′) was 5′-end-labeled to carry out EMSA studies. 10 pmol of unlabeled *tylQ* was mixed with 1× polynucleotide kinase (PNK) buffer (50 mM Tris-HCl (pH 7.6), 10 mM $MgCl_2$, 5 mM dithiothreitol (DTT), and 0.1 mM spermidine). T4 polynucleotide kinase enzyme, 5 units, and [γ-^{32}P]ATP (3300 Ci/mmol) were further added, and the reaction volume was adjusted to 10 μl. After incubating the reaction mixture at 37 °C for 1 h, the enzyme was then deactivated by heating the reaction mixture to 70 °C for 3 min. The labeled product was then purified using the QIAquick nucleotide removal kit protocol provided by Qiagen.

EMSA

Wild-type and mutated (ΔC7, ΔC9, ΔC11, and Triplemut) TylP DNA-binding assays were carried out using the 5′-end-radiolabeled 44-mer *tylQ*. Approximately 10 nM annealed DNA (~5000 cpm) was incubated with 2-fold serially diluted proteins (starting from 10 μM to 150 nM) of the wild-type and all the mutated constructs at 20 °C for 30 min in a buffer containing 20 mM HEPES (pH 7.5), 80 mM NaCl, 15 mM KCl, 0.25 mM EDTA, 0.5 mM DTT, 5% (v/v) glycerol, and 0.2 mg of BSA in a total volume of 20 μl. After the incubation, the samples were run on 6% non-denaturing polyacrylamide gel with 1× TBE as a running buffer (89 mM of both Tris and boric acid and 2 mM EDTA, pH 8.3) at 4 °C and 100 V for 1 h. EMSA results were collected and analyzed on a Storm825, and autoradiograms were generated using the ImageQuantTL software provided by GE Healthcare.

Circular dichroism (CD) studies

The CD experiment was performed with 0.2 mg/ml wild-type and the mutated TylP proteins, and the spectra were taken between the wavelength ranges of 200–260 nm. All the protein samples were prepared in a phosphate buffer (25 mM sodium phosphate, pH 7.5, 80 mM NaCl). Scans were performed at 20 °C using 0.1-cm path length quartz cuvettes with 8 s differential integration time at a scan rate of 50 nm/s.

Molecular dynamics (MD) simulation studies

The initial coordinates of the protein were taken from the native TylP crystal structure. CHARMM-GUI (38), a web-based server, was utilized to generate parameter and topology for the protein and for solvation of the system. The system was solvated with TIP3P water model (39) in a octahedron box having an edge distance of 10 Å from the solute with periodic boundary conditions. The crystal type of the system was considered as an octahedron of 82 Å dimension in *x*, *y*, and *z* direction having a crystal angle of 109.47°. Four potassium ions were added to render the system charge neutral. The total number of particles in the system was 38,819. Charmm36 force-field (40) was used to model all the bonded and non-bonded interactions of the protein atoms. All simulations were performed using the GROMACS 5.0.6 package (41) with Charmm36 all-atom force field. Details of MD studies are provided in supplemental Experimental procedures.

Docking studies

The PDB of the monomeric subunit of different conformations of TylP obtained from MD were used for docking calculations. All docking runs were conducted by using a genetic algorithm in AutoDock version 4.6 (31) against the target ligands. Each ligand for a particular docking run was scored according to a free energy cost function (ΔG^*) that accounts for van der Waals, hydrogen bonding, electrostatic, solvation, and torsional free energy terms. The grid box for docking was selected in the proposed binding pocket region, and rigid docking was performed with 250 runs for each ligand. The top-ranked ligand orientations were selected to identify potential ligands and analyze the interactions in the binding pocket of TylP (supplemental Table S2).

Detailed experimental procedure for ITC, DNA breaking assays using EMSA, and fluorescence quenching studies of TylP are provided in supplemental Experimental procedures.

Author contributions—S. R. conducted most of the experiments, analyzed the results, and wrote part of the paper. A. M. performed the simulation experiments and wrote part of the paper. A. B. performed cloning and purification of TylP. S. P. provided access to synchrotron source for crystal data collection, helped in solving the crystal structure of TylP, and wrote part of the paper. J. M. helped in performing the simulation experiments, analyzed the simulation data, and wrote the simulation part with A. M. R. A. conceived the idea of the project, contributed new reagents/analytical tools, analyzed the results, and wrote most of the paper.

Acknowledgments—We thank all the beamline staff at MX2, Australian Synchrotron, Victoria, Australia, where the diffraction data were collected. We also thank the Protein Crystallography Facility at IIT Bombay for helping with the initial crystallization trials. We thank Prof. Eric Cundliffe (University of Leicester) for providing us with the S. fradiae strain. The molecular dynamic simulation work was funded by an early career research grant.

References

1. Cuthbertson, L., and Nodwell, J. R. (2013) The TetR family of regulators. *Microbiol. Mol. Biol. Rev.* **77,** 440–475
2. Hinrichs, W., Kisker, C., Düvel, M., Müller, A., Tovar, K., Hillen, W., and Saenger, W. (1994) Structure of the Tet repressor-tetracycline complex and regulation of antibiotic resistance. *Science* **264,** 418–420
3. Hernández, A., Maté, M. J., Sánchez-Díaz, P. C., Romero, A., Rojo, F., and Martínez, J. L. (2009) Structural and functional analysis of SmeT, the repressor of the *Stenotrophomonas maltophilia* multidrug efflux pump SmeDEF. *J. Biol. Chem.* **284,** 14428–14438
4. Bassler, B. L., and Losick, R. (2006) Bacterially speaking. *Cell* **125,** 237–246
5. Davies, J., and Davies, D. (2010) Origins and evolution of antibiotic resistance. *Microbiol. Mol. Biol. Rev.* **74,** 417–433
6. Liu, G., Chater, K. F., Chandra, G., Niu, G., and Tan, H. (2013) Molecular regulation of antibiotic biosynthesis in *Streptomyces*. *Microbiol. Mol. Biol. Rev.* **77,** 112–143
7. Sengupta, S., Chattopadhyay, M. K., and Grossart, H.-P. (2013) The multifaceted roles of antibiotics and antibiotic resistance in nature. *Front. Microbiol.* **4,** 47
8. Fishman, S. E., Cox, K., Larson, J. L., Reynolds, P. A., Seno, E. T., Yeh, W. K., Van Frank, R., and Hershberger, C. L. (1987) Cloning genes for the biosynthesis of a macrolide antibiotic. *Proc. Natl. Acad. Sci. U.S.A.* **84,** 8248–8252
9. Bignell, D. R., Bate, N., and Cundliffe, E. (2007) Regulation of tylosin production: role of a TylP-interactive ligand. *Mol. Microbiol.* **63,** 838–847
10. Bate, N., Butler, A. R., Gandecha, A. R., and Cundliffe, E. (1999) Multiple regulatory genes in the tylosin biosynthetic cluster of *Streptomyces fradiae*. *Chem. Biol.* **6,** 617–624
11. Fouces, R., Mellado, E., Díez, B., and Barredo, J. L. (1999) The tylosin biosynthetic cluster from *Streptomyces fradiae*: genetic organization of the left region. *Microbiology* **145,** 855–868
12. Stratigopoulos, G., Gandecha, A. R., and Cundliffe, E. (2002) Regulation of tylosin production and morphological differentiation in *Streptomyces fradiae* by TylP, a deduced γ-butyrolactone receptor. *Mol. Microbiol.* **45,** 735–744
13. Onaka, H., Nakagawa, T., and Horinouchi, S. (1998) Involvement of two A-factor receptor homologues in *Streptomyces coelicolor* A3(2) in the regulation of secondary metabolism and morphogenesis. *Mol. Microbiol.* **28,** 743–753
14. Williamson, N. R., Fineran, P. C., Leeper, F. J., and Salmond, G. P. (2006) The biosynthesis and regulation of bacterial prodiginines. *Nat. Rev. Microbiol.* **4,** 887–899

15. Biswas, A., Swarnkar, R. K., Hussain, B., Sahoo, S. K., Pradeepkumar, P. I., Patwari, G. N., and Anand, R. (2014) Fluorescence quenching studies of γ-butyrolactone binding protein (CprB) from *Streptomyces coelicolor* A3(2). *J. Phys. Chem. B* **118,** 10035–10042
16. Natsume, R., Ohnishi, Y., Senda, T., and Horinouchi, S. (2004) Crystal structure of a γ-butyrolactone autoregulator receptor protein in *Streptomyces coelicolor* A3(2). *J. Mol. Biol.* **336,** 409–419
17. Yamazaki, H., Ohnishi, Y., and Horinouchi, S. (2000) An A-factor-dependent extracytoplasmic function sigma factor (σAdsA) that is essential for morphological development in *Streptomyces griseus*. *J. Bacteriol.* **182,** 4596–4605
18. Xu, G., Wang, J., Wang, L., Tian, X., Yang, H., Fan, K., Yang, K., and Tan, H. (2010) "Pseudo" γ-butyrolactone receptors respond to antibiotic signals to coordinate antibiotic biosynthesis. *J. Biol. Chem.* **285,** 27440–27448
19. Ramos, J. L., Martínez-Bueno, M., Molina-Henares, A. J., Terán, W., Watanabe, K., Zhang, X., Gallegos, M. T., Brennan, R., and Tobes, R. (2005) The TetR family of transcriptional repressors. *Microbiol. Mol. Biol. Rev.* **69,** 326–356
20. Bhukya, H., Bhujbalrao, R., Bitra, A., and Anand, R. (2014) Structural and functional basis of transcriptional regulation by TetR family protein CprB from *S. coelicolor A3*(*2*). *Nucleic Acids Res.* **42,** 10122–10133
21. Schumacher, M. A., Miller, M. C., Grkovic, S., Brown, M. H., Skurray, R. A., and Brennan, R. G. (2001) Structural mechanisms of QacR induction and multidrug recognition. *Science* **294,** 2158–2163
22. Le, T. B., Schumacher, M. A., Lawson, D. M., Brennan, R. G., and Buttner, M. J. (2011) The crystal structure of the TetR family transcriptional repressor SimR bound to DNA and the role of a flexible N-terminal extension in minor groove binding. *Nucleic Acids Res.* **39,** 9433–9447
23. Itou, H., Watanabe, N., Yao, M., Shirakihara, Y., and Tanaka, I. (2010) Crystal structures of the multidrug binding repressor *Corynebacterium glutamicum* CgmR in complex with inducers and with an operator. *J. Mol. Biol.* **403,** 174–184
24. Liang, J., Edelsbrunner, H., and Woodward, C. (1998) Anatomy of protein pockets and cavities: measurement of binding site geometry and implications for ligand design. *Protein Sci.* **7,** 1884–1897
25. Hernández, A., Ruiz, F. M., Romero, A., and Martínez, J. L. (2011) The binding of triclosan to SmeT, the repressor of the multidrug efflux pump SmeDEF, induces antibiotic resistance in *Stenotrophomonas maltophilia*. *PLoS Pathog.* **7,** e1002103
26. Veal, W. L., Nicholas, R. A., and Shafer, W. M. (2002) Overexpression of the MtrC-MtrD-MtrE efflux pump due to an mtrR mutation is required for chromosomally mediated penicillin resistance in *Neisseria gonorrhoeae*. *J. Bacteriol.* **184,** 5619–5624
27. Fujihashi, M., Nakatani, T., Hirooka, K., Matsuoka, H., Fujita, Y., and Miki, K. (2014) Structural characterization of a ligand-bound form of *Bacillus subtilis* FadR involved in the regulation of fatty acid degradation. *Proteins* **82,** 1301–1310
28. Collaborative Computational Project No 4. (1994) The CCP4 suite: programs for protein crystallography. *Acta Crystallogr. D Biol. Crystallogr.* **50,** 760–763
29. Premkumar, L., Rife, C. L., Sri Krishna, S., McMullan, D., Miller, M. D., Abdubek, P., Ambing, E., Astakhova, T., Axelrod, H. L., Canaves, J. M., Carlton, D., Chiu, H. J., Clayton, T., DiDonato, M., Duan, L., *et al.* (2007) Crystal structure of TM1030 from *Thermotoga maritima* at 2.3 A resolution reveals molecular details of its transcription repressor function. *Proteins* **68,** 418–424
30. Bhukya, H., and Anand, R. (2017) TetR regulators: a structural and functional perspective. *J. Ind. Inst. Sci.* **97,** 245–259
31. Morris, G. M., Huey, R., Lindstrom, W., Sanner, M. F., Belew, R. K., Goodsell, D. S., and Olson, A. J. (2009) AutoDock4 and AutoDockTools4: Automated docking with selective receptor flexibility. *J. Comput. Chem.* **30,** 2785–2791
32. Zheng, J., Sagar, V., Smolinsky, A., Bourke, C., LaRonde-LeBlanc, N., and Cropp, T. A. (2009) Structure and function of the macrolide biosensor protein, MphR(A), with and without erythromycin. *J. Mol. Biol.* **387,** 1250–1260
33. Bate, N., Stratigopoulos, G., and Cundliffe, E. (2002) Differential roles of two SARP-encoding regulatory genes during tylosin biosynthesis. *Mol. Microbiol.* **43,** 449–458
34. Saghai-Maroof, M. A., Soliman, K. M., Jorgensen, R. A., and Allard, R. W. (1984) Ribosomal DNA spacer-length polymorphisms in barley: mendelian inheritance, chromosomal location, and population dynamics. *Proc. Natl. Acad. Sci. U.S.A.* **81,** 8014–8018
35. Panjikar, S., Parthasarathy, V., Lamzin, V. S., Weiss, M. S., and Tucker, P. A. (2005) Auto-Rickshaw: an automated crystal structure determination platform as an efficient tool for the validation of an X-ray diffraction experiment. *Acta Crystallogr. D Biol. Crystallogr.* **61,** 449–457
36. Emsley, P., and Cowtan, K. (2004) Coot: model-building tools for molecular graphics. *Acta Crystallogr. D Biol. Crystallogr.* **60,** 2126–2132
37. Delano, W. L. (2002) *The PyMOL Molecular Graphics System*. Version 1.8.2.0. DeLano Scientific LLC, San Carlos, CA
38. Jo, S., Kim, T., Iyer, V. G., and Im, W. (2008) CHARMM-GUI: a web-based graphical user interface for CHARMM. *J. Comput. Chem.* **29,** 1859–1865
39. Jorgensen, W. L., and Madura, J. D. (1983) Quantum and statistical mechanical studies of liquids. 25. Solvation and conformation of methanol in water. *J. Am. Chem. Soc.* **105,** 1407–1413
40. Best, R. B., Zhu, X., Shim, J., Lopes, P. E., Mittal, J., Feig, M., and Mackerell, A. D., Jr. (2012) Optimization of the additive CHARMM all-atom protein force field targeting improved sampling of the backbone ϕ, ψ and side-chain $\chi(1)$ and $\chi(2)$ dihedral angles. *J. Chem. Theory Comput.* **8,** 3257–3273
41. Van Der Spoel, D., Lindahl, E., Hess, B., Groenhof, G., Mark, A. E., and Berendsen, H. J. (2005) GROMACS: fast, flexible, and free. *J. Comput. Chem.* **26,** 1701–1718

Functional insights into the mode of DNA and ligand binding of the TetR family regulator TylP from *Streptomyces fradiae*

Shamayeeta Ray, Anwesha Maitra, Anwesha Biswas, Santosh Panjikar, Jagannath Mondal and Ruchi Anand

J. Biol. Chem. 2017, 292:15301-15311.
doi: 10.1074/jbc.M117.788000 originally published online July 24, 2017